

Vanishing Compactness Gap and Fermionic Compact Dark Matter in Hořava-Lifshitz Gravity

Edwin J. Son,^{1,*} Kyungmin Kim,^{2,†} and John J. Oh^{1,‡}

¹*National Institute for Mathematical Sciences, Daejeon 34047, Republic of Korea*

²*Korea Astronomy and Space Science Institute, Daejeon 34055, Republic of Korea*

(Dated: January 27, 2026)

We show that the gap in the compactness between black holes and neutron stars witnessed in general relativity may be vanishing in Hořava-Lifshitz (HL) gravity. Assuming a fermion equation-of-state for simplicity, and solving the Tolman-Oppenheimer-Volkoff equation within the HL gravity framework, we see that there exists a minimum fermion mass $m_f^{(\min)}(q, y)$, above which the gap of the compactness between black hole and fermionic compact object vanishes, for a given deformation parameter q of HL and interaction strength y between fermions. Thus, in HL gravity, the mass and radius of an object found in the lower mass gap by LIGO-Virgo-KAGRA observations might not be able to classify it as a black hole or a neutron star. It is interesting to note that a fermion of mass ~ 40 GeV can form a highly compact object of mass $\sim 10^{-4} M_\odot$ and radius ~ 1 m that may play the role of the cold dark matter. In addition, we find the possible existence of another class of compact objects whose compactness is comparable to that of a black hole.

I. INTRODUCTION

Hořava-Lifshitz (HL) gravity [1–3] has been proposed as a framework in which gravitational dynamics can vary with the energy scale. While general relativity (GR) successfully describes gravity at macroscopic scales, it fails to remain renormalizable in the ultraviolet (UV) regime, where quantum effects become unavoidable for example, in the early Universe or near black hole (BH) horizon. A renormalizable theory of gravity is therefore expected to exhibit improved behavior at high energies and short distances. HL gravity approaches this challenge by abandoning local Lorentz invariance at high energies and introducing an anisotropic scaling between time and space, reminiscent of Lifshitz-type theories in condensed-matter physics. This scaling modification is crucial for achieving power-counting renormalizability, even though it explicitly breaks Lorentz symmetry in the UV regime. Importantly, HL gravity is constructed so that GR is recovered in the infrared (IR) limit, ensuring consistency with well-tested low-energy gravitational phenomena. Since its inception, HL gravity has inspired extensive research across cosmology [4], BH physics [5, 6], and quantum gravity as a candidate UV-complete theory of gravitation [7].

In particular, the deformed HL gravity can be treated as a special model since it possesses an asymptotically Minkowskian structure while exhibiting modifications in the UV regime [2, 8]. In Ref. [9], the authors investigated the static configurations of neutron star (NS)-like objects with several representative equation-of-state (EOS) in the deformed HL gravity, finding that the maximum stable mass and radius become larger than those in GR due to the effectively weaker gravitational interaction in the UV region. This naturally raises a question: *Can purely fermionic matter form compact objects with NS-scale masses in the deformed HL framework?*

Meanwhile, in GR, there exists a gap in the allowed values of the compactness M/R with $c = G = 1$, where M and R denote the mass and radius of a self-gravitating system, respectively. The compactness of a Schwarzschild BH is always 0.5, while that of a typical NS is predicted as about 0.1–0.2 [10–12], regarding possible channels for producing each type of compact objects. The theoretical maximum of a NS is about 0.3 [11, 12] and no compact object can be formed with compactness between 0.3 and 0.5 in GR.¹ This naturally provokes another question: *Is the compactness gap itself a universal prediction of gravity models, or is it a theory-dependent effective phenomenon?*

In relation to the compactness gap defined theoretically, there exists observational evidence of the so-called *lower mass gap* between NSs and BHs, typically in the range of $3 M_\odot$ to $5 M_\odot$ [15–17].² As an example, the primary mass of the compact binary system associated with the gravitational-wave event, GW230529_181500, has been inferred to be 2.5 – $4.5 M_\odot$ [18]. Relevant studies [19–24] discuss the possibility that objects within the observed mass gap may result from binary merger processes, rather than originating from isolated stellar evolution. However, the merger rate of a NS and the remnant of a binary neutron star merger is several orders of magnitude lower than the rate inferred for the event like GW230529_181500 [18]. Therefore, a debate about the unresolved lower mass gap in astrophysical observations—closely related to the compactness gap in GR—is still ongoing.

Motivated by this, we demonstrate that the compactness gap between NSs and BHs can vanish in the framework of deformed HL gravity. By solving the Tolman-Oppenheimer-Volkoff (TOV) equations [10, 25] for fermionic matter within the framework of deformed HL gravity, we show that there ex-

¹ Though the upper bound in the compactness of charged compact objects for a Reissner-Nordström vacuum is $8/9$ [13, 14], the observed NSs are charge neutral so that such charged compact objects are not under consideration in this work. In addition, we only consider non-rotating objects for simplicity.

² Note that the lower ends of both the compactness gap and the mass gap correspond to the maximum mass (or maximum compactness) of NSs in GR.

* eddy@nims.re.kr
† kkim@kasi.re.kr
‡ johnoh@nims.re.kr

ist stable compact configurations whose mass and radius approach those of the minimal Kehagias-Sfetsos (KS) BH [5], thereby continuously filling the gap in compactness. This result suggests that, once gravity is modified, the notion of a compactness gap may not be guaranteed, and that compact objects with compactness comparable to BHs can be supported without forming an event horizon. As a consequence, compact objects lying in the compactness gap could be interpreted as exotic compact objects arising from modified gravity.

Furthermore, for certain ranges of fermion masses and interaction strengths, such highly compact configurations may also appear at sub-solar masses, which suggests that they could constitute a viable class of compact dark matter (DM) candidates. Specifically, our results indicate that the vanishing compactness gap represents a distinctive strong-field astrophysical signature of HL gravity beyond GR, with potential implications for both gravitational-wave observations and DM phenomenology. Therefore, comparing fermionic compact DM in GR [26–29] with its counterpart in the deformed HL gravity may shed light on the viability of modified gravity as a DM candidate.

We organize this paper as follows: In Sec. II, we briefly introduce the deformed HL gravity model and the corresponding TOV equation and summarize the equation of state model that we are considering. In Sec. III, we present the result of numerical study performed for the compactness gap and the fermionic cold DM candidates. In Sec. IV, we discuss the results and present the future prospects.

II. TOV EQUATION IN HL GRAVITY

A. Equations of motion in HL gravity

The action of HL gravity is formulated by an anisotropic scaling between time and space, $t \rightarrow b^z t$ and $x^i \rightarrow b x^i$ and the form of $z = 3$:

$$I_{\text{HL}} = \int dt d^3x \sqrt{g} N \left[\frac{2}{\kappa^2} (\mathcal{K}_{ij} \mathcal{K}^{ij} - \lambda \mathcal{K}^2) - \frac{\kappa^2}{2\zeta^4} \left(\mathcal{C}_{ij} - \frac{\mu\zeta^2}{2} \mathcal{R}_{ij} \right) \left(\mathcal{C}^{ij} - \frac{\mu\zeta^2}{2} \mathcal{R}^{ij} \right) + \frac{\kappa^2 \mu^2 (4\lambda - 1)}{32(3\lambda - 1)} \left(\mathcal{R}^2 + \frac{2}{(4\lambda - 1)q^2} \mathcal{R} + \frac{12\Lambda_W^2}{4\lambda - 1} \right) \right] \quad (1)$$

with the *softly* broken detailed balance condition, which is sometimes called the deformed HL gravity in the literature [1–3, 8]. Note that $\mathcal{K}_{ij} \equiv \frac{1}{2N} [\dot{g}_{ij} - \nabla_i N_j - \nabla_j N_i]$ is an extrinsic curvature, where N is a lapse function, N^i is a shift vector, g_{ij} is a three-dimensional spatial metric, and \dot{g}_{ij} denotes $\partial g_{ij} / \partial t$. $\mathcal{C}^{ij} \equiv \varepsilon^{ik\ell} \nabla_k (\mathcal{R}_\ell^j - \delta_\ell^j \mathcal{R}/4)$ is a Cotton-York tensor, where \mathcal{R}_{ij} and \mathcal{R} are a three-dimensional spatial Ricci tensor and a Ricci scalar, respectively. κ^2 is a coupling constant related to the Newton's gravitational constant G_N , and λ is an additional dimensionless coupling constant characterizing deviations from GR in the kinetic term of HL gravity. Here, q is essential for an asymptotically flat solution, though

it violates the detailed balance condition. The coupling constants μ , Λ_W , and ζ stem from the three-dimensional Euclidean topologically massive gravity action [30, 31]. When $\lambda = 1$, the Einstein-Hilbert action can be recovered in the infrared (IR) limit by identifying the fundamental constants with $c = (\kappa^2/4)[\mu^2/2q^2(3\lambda - 1)]^{1/2}$, $G_N = \kappa^2 c^2 / 32\pi$, and $\Lambda = -3q^2 \Lambda_W^2$, representing the speed of light, Newton's gravitational constant, and the cosmological constant, respectively.

The total action under consideration is given by $I_{\text{tot}} = I_{\text{HL}} + I_{\text{mat}}$, where I_{mat} represents the matter action that will be specified by assuming a perfect fluid and choosing an EOS without an explicit form. Hereafter, we consider $c = G_N = 1$ and an asymptotically flat geometry, that is, $\Lambda = 0$, for simplicity.

Now, if we consider a static, spherically symmetric metric ansatz,

$$ds^2 = -e^{2\Phi(r)} dt^2 + \frac{dr^2}{f(r)} + r^2 (d\theta^2 + \sin^2 \theta d\phi^2), \quad (2)$$

then the equations of motion in HL gravity with the stress-energy tensor of a perfect fluid, $T_{\mu\nu} = (\rho + p)u_\mu u_\nu + p g_{\mu\nu}$, are given by

$$\rho = \frac{q^2}{8\pi r^2} \left(\frac{r}{q^2} (1 - f) + \frac{(1 - f)^2}{r} \right)', \quad (3a)$$

$$p = \frac{q^2}{8\pi r^4} \left[(1 - f) \left(1 - f - \frac{r^2}{q^2} \right) + 4rf \left(1 - f + \frac{r^2}{2q^2} \right) \Phi' \right], \quad (3b)$$

$$p' = -(\rho + p) \Phi', \quad (3c)$$

where $u_\mu = (1, 0, 0, 0)$ is a four-vector field, ρ and p are the energy density and the pressure of a perfect fluid, respectively, and the prime denotes d/dr . Note that HL gravity has six parameters, as observed in Eq. (1): we have already fixed λ and Λ_W to 1 and 0, respectively, κ and μ are hidden in the physical constants related to c and G_N in the IR region, and ζ does not contribute to this non-rotating configuration. Thus, q is the only remaining free parameter of the theory.

Following the procedure in Ref. [32] to solve Eq. (3), we replace $f(r)$ by $m(r)$ through the relation

$$f = \frac{1 - 2m/r + q^2/r^2}{2^{-1} \left[1 + 2q^2/r^2 + \sqrt{1 + 8q^2mr^{-3}} \right]}. \quad (4)$$

Note that the numerator is the same form of the Reissner-Nordström vacuum, when $m(r) = M$ and $q = Q$, which reminds us that the noncommutative Schwarzschild BH behaves like the Reissner-Nordström BH in thermodynamic analysis [33]. Similar to the Reissner-Nordström vacuum, the horizons of the KS BH are located at $r_\pm = M \pm \sqrt{M^2 - M_c^2}$, where $M_c \equiv |q|$ is the critical mass for horizon formation [5].

However, in the limit of $q/r \ll 1$, the metric function (4) approximates $f \approx 1 - 2M/r + 4q^2 M^2/r^4 + \mathcal{O}(q/r)^4$ so that it converges to the Schwarzschild vacuum either in the GR

limit ($q \rightarrow 0$) or in IR limit ($r \rightarrow \infty$) where the HL correction terms are negligible. Here, the mass parameter M is identified as the quasilocal energy at infinity [34]. For the KS solution, we see $e^{2\Phi(r)} = f(r)$, while Eq. (3c) governs the behavior of the (tt) -component of the metric, which is coupled to matter in the generic case.

With the Planck mass m_P and length l_P , M_c can be rewritten as $M_c = |q|m_P/\ell_P$, which reduces to $M_c = m_P$ for $|q| = \ell_P$ and becomes $M_c \approx M_\odot$ for $|q| \approx 1.477 \times 10^3$ m, where M_\odot represents the solar mass. For a constant q , the BH horizon exists with $M \geq M_c$.³ On the other hand, for a fixed M , one finds $|q| \leq q_c \equiv M$ to form a BH. Hence, the horizon of a solar mass KS BH exists only if $|q| \leq q_c \approx 1.477 \times 10^3$ m. Considering the possibility of the existence of $\gtrsim 3 M_\odot$ BH, we assume $|q| \lesssim 4.5 \times 10^3$ m. Accordingly, in this study we restrict the range of the parameter as $|q| \leq 4 \times 10^3$ m.

B. TOV equations for fermionic gas

Now, we can rewrite Eq. (3) as follows:

$$m' = 4\pi r^2 \rho, \quad (5a)$$

$$p' = -\frac{m\rho\mathfrak{A}}{r^2\mathfrak{B}} \frac{(1+p/\rho)[1+4\pi r^3 p\mathfrak{B}/m - q^2\tilde{\rho}]}{\sqrt{1+8q^2\tilde{\rho}}[1-2m/r+q^2/r^2]}, \quad (5b)$$

where $\mathfrak{A} = 2^{-1}[1+2q^2/r^2 + \sqrt{1+8q^2\tilde{\rho}}]$, $\mathfrak{B} = 2^{-1}[1+2q^2\tilde{\rho} + \sqrt{1+8q^2\tilde{\rho}}]$, and $\tilde{\rho} = mr^{-3}$. Note that if we expand p' in terms of $q \rightarrow 0$ and take the leading order, we obtain

$$p' \approx -\frac{m\rho}{r^2} \left(1 + \frac{p}{\rho}\right) \left(1 + \frac{4\pi r^3 p}{m}\right) \left(1 - \frac{2m}{r}\right)^{-1}, \quad (6)$$

which reproduces the TOV equation in GR.

The EOS for a free fermion gas at zero temperature is given by the energy density ρ and the pressure p , defined as

$$\rho = \frac{1}{\pi^2} \int_0^{k_F} k^2 \sqrt{m_f^2 + k^2} dk = \frac{m_f^4}{8\pi^2} [(2\eta^3 + \eta)(1 + \eta^2)^{1/2} - \sinh^{-1}(\eta)], \quad (7)$$

$$p = \frac{1}{3\pi^2} \int_0^{k_F} \frac{k^4}{\sqrt{m_f^2 + k^2}} dk = \frac{m_f^4}{24\pi^2} [(2\eta^3 - 3\eta)(1 + \eta^2)^{1/2} + 3\sinh^{-1}(\eta)], \quad (8)$$

where k_F is the Fermi momentum, m_f is the mass of a fermion, and η is the dimensionless Fermi momentum defined as $\eta \equiv k_F/m_f$.

In a more realistic treatment, it is natural to introduce interactions between fermions. To this end, we follow the approach of [26], in which two-body interaction terms are added to both Eqs. (7) and (8) as

$$\rho_{\text{int}} = \left(\frac{m_f^2}{3\pi^2}\right)^2 y^2 \eta^6, \quad p_{\text{int}} = \left(\frac{m_f^2}{3\pi^2}\right)^2 y^2 \eta^6, \quad (9)$$

where $y = m_f/m_I$ parametrizes the interaction strength, with m_I denoting the interaction energy scale.

III. NUMERICAL SOLUTIONS FOR FERMIONIC COMPACT OBJECTS IN HL GRAVITY

A. Fermion of neutron mass

To obtain the mass-radius relation of fermionic compact objects in HL gravity (Fig. 1), we numerically solve the TOV equation in Eq. (5) while varying the central energy density, ρ_c , for three selected values of the parameter q : 0 m, 400 m, and 4 000 m.⁴ In addition, the sound speed limit for KS vacuum in the figure is obtained by restricting the sound speed inside the object less than or equal to the speed of light c , which is referred to as the causal limit in GR [32]. We find that all the stable compact objects are well formed below the sound speed limit curve.

As shown in the case (a) of Fig. 1, solving the TOV equation in GR—the TOV equation in HL gravity with $q = 0$, equivalently—shows that a compact object supported by a free fermionic gas of neutron-like fermions (~ 1 GeV) has a maximum mass below one solar mass, whereas the inclusion of interactions among the fermions increases both the maximum mass and the radius. [10, 26] Here, we take $y = 10$ as an example. For comparison, the mass-radius profile for a NS EOS, Akmal-Pandharipande-Ravenhall (APR4) [40], is also presented.

In HL gravity, i.e., for $q \neq 0$, considering the same fermion mass as that of neutron, the resulting mass-radius relations of fermionic compact objects are shown in the cases (b) and (c) of Fig. 1: For the case of (b) $q = 400$ m, the behavior of compact objects is almost the same as that of GR. The main difference is exhibited on the left branch beyond the maximum point (the most massive compact object), which is unstable and thus unphysical as an equilibrium solution. However, for the case of (c) $q = 4 000$ m, the maximum mass is significantly larger than that in GR. Furthermore, the mass and the size of the most massive compact object of free fermion are almost the same as those of the minimal KS BH. It is plausible that HL gravity allows such objects which may not be distinguishable from BHs with current observational capabilities. We will look into it in the following section.

³ When $M < M_c$, a naked singularity appears, and the detailed behavior of the formation of naked singularities and wormholes in Hořava gravity is studied in [35, 36]. In the quantum regime, however, the KS geometry turns out to be regular [37], which may safely avoid the naked singularity problem.

⁴ In solving the TOV equation, as done in [32], we employ the eighth-order Runge-Kutta method [38] implemented in SciPy [39].

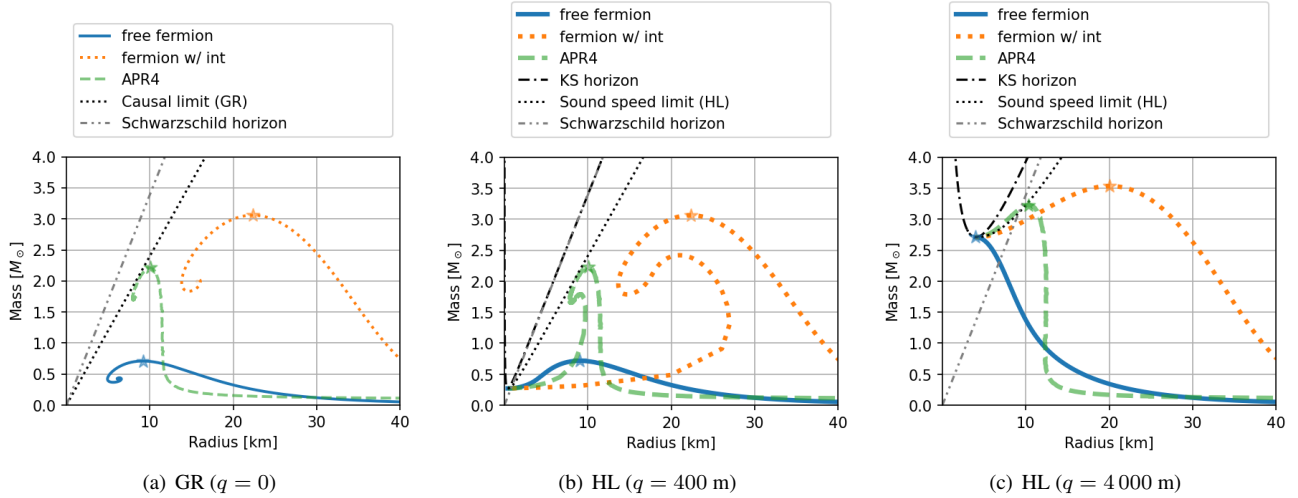


FIG. 1. Comparison of fermionic compact objects of $m_f = m_n$ with and without interaction term and compact object whose EOS is APR4 in (a) GR and (b,c) HL. The blue solid curves represent compact objects made of free fermions, the orange dotted curves represent fermionic compact objects with two-body interactions, and the green dashed curves are the compact objects with the APR4 EOS. The horizons of the KS and Schwarzschild BHs are also plotted as the dash-dotted and dash-double dotted curves, respectively. The sound speed limit (causal limit) of KS and Schwarzschild vacua are depicted as dotted curves, respectively.

B. Arbitrary q and various m_f

We now consider an arbitrarily nonzero q , keeping the above constraints, of course, and introduce dimensionless mass $M/|q|$ and radius $R/|q|$. Then, the most massive stable compact objects of q -independent mass-radius profiles can be plotted in Fig. 2: Each point represents the most massive compact object when a fermion mass m_f and an interaction strength y are given, which are distinguished by the position and the marker shape, respectively. Specifically, for a given y , the point of smaller values in both $M/|q|$ and $R/|q|$ indicates the case of more massive m_f . From this figure, we find that all the most massive objects are formed below the sound speed limit curve [32]—obtained in analogy with the calculation of the causal limit in GR [11, 12]. Then, it is implied that the causality remains satisfied for compact objects in HL.

It is interesting to note that R goes to $|q|$, as m_f becomes larger, and the most massive objects of all considered values of the interaction strength y come closer to the KS horizon and eventually reach the minimal BH point. In other words, for an arbitrary q , there may exist a compact object whose mass and radius are similar to the minimal BH, $M \sim |q| \sim R$. However, we find no significant difference among the most massive objects of different nonzero y 's except for the case $y = 0$. From this result, we understand that the m_f -dependent profile mainly relies on whether $y = 0$ or not.

To see the properties of such objects, we investigate the compactness M/R with respect to the fermion mass m_f and the central density ρ_c (Fig. 3). The compactness of the KS BH is in the range of $1/2 < M/R \leq 1$: The large KS BHs ($r_+ \gg |q|$) is approximated to Schwarzschild BHs and the small KS BHs is bounded by the minimal BH $r_+^{\min} = M_{\text{BH}}^{\min} = |q|$. As mentioned above, fermionic compact objects can be

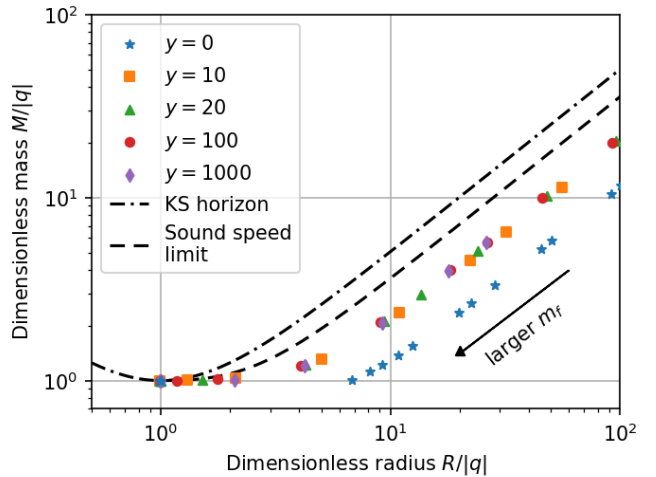


FIG. 2. Comparison of fermionic compact objects with and without two-body interaction term in EOS for some interaction strengths y and various fermion masses m_f . For a given y , the point of smaller $M/|q|$ and $R/|q|$ indicates the case of more massive m_f . All the most massive stable objects are below the sound speed limit (causal limit) in KS vacuum.

formed with the masses and radii similar to those of the minimal BH, and hence their compactness is bounded from above, $M/R < 1$.

As shown in Fig. 3(a), the fermion mass scale for a compact object to attain a compactness within the KS BHs range depends on the interaction strength y , as summarized in Table I. The scales in the table look somewhat high, but higher q reduces the values to reasonable scales. For example, considering $q \sim 4000$ m, the mass scales in Table I are multiplied

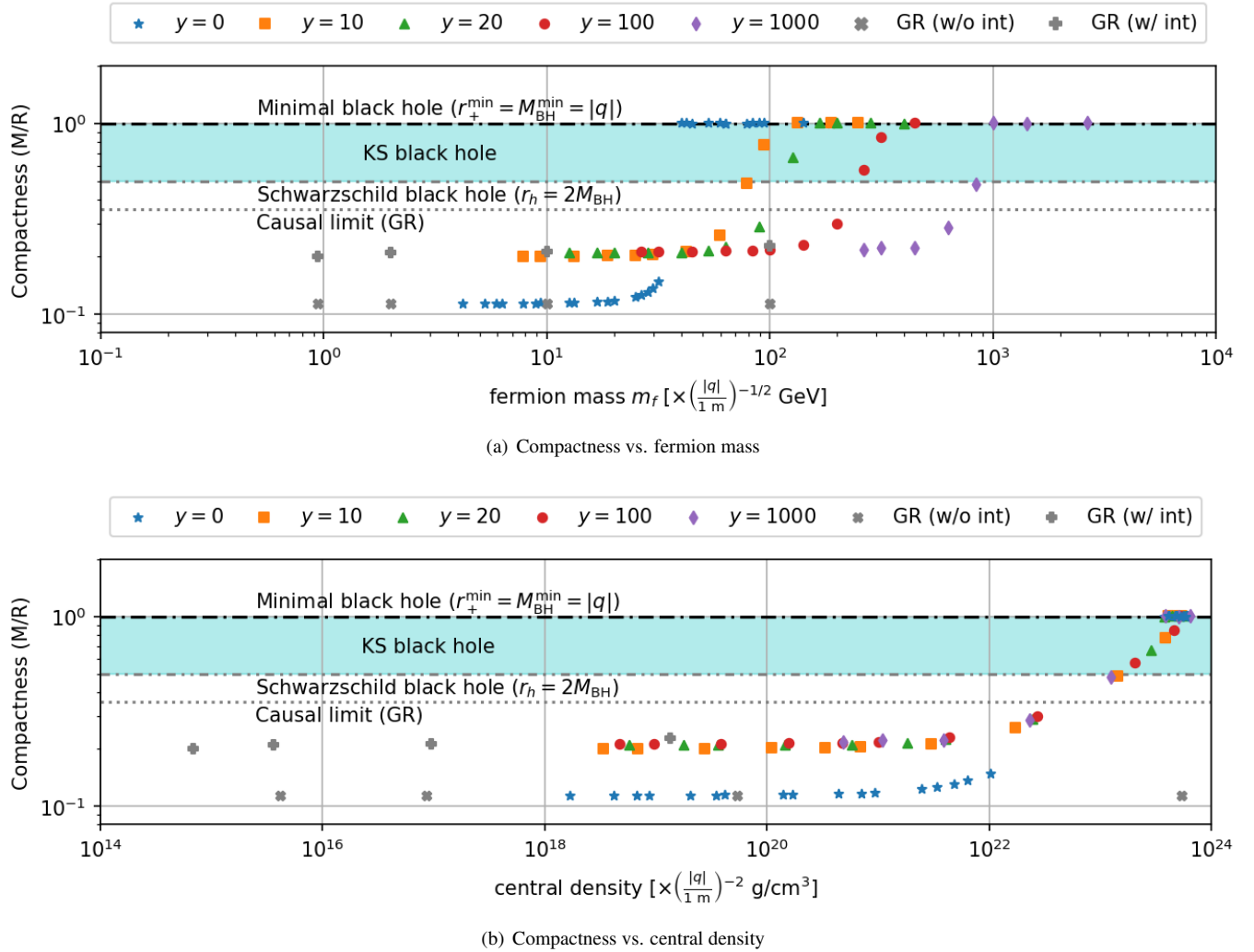


FIG. 3. Compactness of the most massive fermionic compact objects in HL gravity for several interaction strengths y are depicted with respect to (a) various fermion masses m_f and (b) various central densities ρ_c . Compactness of several fermionic compact objects in GR with interaction energy $m_I \sim 100$ MeV are also shown in dimension (a) [GeV] and (b) [g/cm^3] for comparison. The compactness of a KS BH is between that of a Schwarzschild BH, $1/2$, and that of a minimal BH, 1 , according to the ratio of $|q|/M_{\text{BH}}$, and it is represented by the shaded region. The compactness of sound speed limit of KS vacuum is also between that of causal limit of Schwarzschild vacuum in GR and that of a minimal BH, according to the ratio of $|q|/R$.

by a factor $\sim 1/60$ and reduce to $\sim 0.6\text{--}16$ GeV.

In Fig. 3(b), we plot the compactness M/R of the most massive fermionic compact objects in HL gravity as a function of the central density ρ_c for several interaction strength y . For a given y , the compactness increases monotonically with increasing central density, reflecting the formation of progressively denser equilibrium configurations. It is interesting to note that the central density of a fermionic compact object with compactness $1/2 \leq M/R \leq 1$ is given by $\sim 10^{23} \times (|q|/1 \text{ m})^{-2} \text{ g}/\text{cm}^3$ for all y , which reduces to $\sim 10^{16} \text{ g}/\text{cm}^3$ for $q \sim 4000 \text{ m}$. Note that this critical central density is universal in the sense that it is independent of the interaction strength y .

We see in Fig. 3 that the compactness of a compact object approaches the range allowed for KS black holes, when

TABLE I. The mass scale of the fermion for a compact object to have its compactness in the range of that of KS BHs depends on the interaction strength y .

interaction strength y	fermion mass $m_f [\times (q /1 \text{ m})^{-1/2} \text{ GeV}]$
0	40
10	80
20	120
100	300
1 000	1 000

its fermion mass m_f is larger than the y -dependent value given in Table I and its central density is given by $\rho_c \gtrsim 10^{23} \times (|q|/1 \text{ m})^{-2} \text{ g}/\text{cm}^3$. In comparison with fermionic compact objects in GR, the solutions in HL gravity exhibit a

systematically higher upper bound on the compactness, indicating that stable equilibrium configurations with larger compactness can be supported in higher m_f and ρ_c . This behavior suggests that considering an exotic particle of higher m_f and ρ_c or considering a large q in the HL gravity allows us to expect equilibrium structures which can vanish the compactness gap in GR.

C. Compact dark matter candidate in HL gravity

A smaller q leads to a smaller minimal BH and the compactness of fermionic compact objects is bounded from above $M/R < 1$. Hence, in this section, we focus on smaller $q \leq 1$ m and examine the mass of corresponding compact object.

For the case of $q \sim 1$ m, the radius and mass of the minimal BH are $r_+^{\min} = 1$ m and $M_{\text{BH}}^{\min} \sim 10^{-4} M_\odot$, respectively, which corresponds to the cold DM candidate [26]. Although this mass of primordial BH has been excluded as constituting the majority of cold DM, it may still survive as a subdominant component of DM (see Ref. [41] and references therein). For the case of $q \sim 1$ nm, on the other hand, it alone may account for the entire DM abundance, since the mass becomes $M_{\text{BH}}^{\min} \sim 10^{-13} M_\odot$.

Meanwhile, regarding the Hawking temperature $T_H = (4\pi r_+)^{-1}(r_+^2 - q^2)/(r_+^2 + 2q^2)$ [42], we expect that the minimal BH does not evaporate, namely, $T_H = 0$ because $r_+ = |q|$. Therefore, there may be a population of (near-)minimal BHs in the Universe as remnants of the evaporation of primordial BHs. Moreover, no radiation of minimal BH and faint radiation of near-minimal BH push the lower bound of the mass of primordial BH even lower. This implies that much smaller q (i.e. much smaller minimal BH), is available as a cold DM candidate, which would be challenging to detect with current observational techniques such as microlensing.

In the same manner, a fermionic compact object can have similar mass and radius to those of the minimal BH when m_f is high enough and ρ_c is close to $10^{24} \times (|q|/1 \text{ m})^{-2} \text{ g/cm}^3$. Then, if q is small enough, it is naturally expected that tiny fermionic compact objects of $M \sim M_{\text{BH}}^{\min} \ll 1 M_\odot$ can be formed. In addition, a compact object of compactness ~ 1 may play the role of a cold DM candidate, since it does not evaporate and its small size allow it to survive without fatal interactions. Thus, both the (near-)minimal BHs and tiny fermionic compact objects may contribute to DM.

IV. DISCUSSIONS

Consequently, both the (near-)minimal BHs and the compact objects of compactness ~ 1 are capable of playing the role of DM. Moreover, for $q \sim 1$ nm, the mass of the minimal BH becomes $M_{\text{BH}}^{\min} \sim 10^{-13} M_\odot$ and the compact object at this scale remains essentially unconstrained by current observation. However, at this small scale of q , the fermion mass scale in Table I increases dramatically to $\sim 120 \text{ TeV} - 3 \text{ PeV}$,

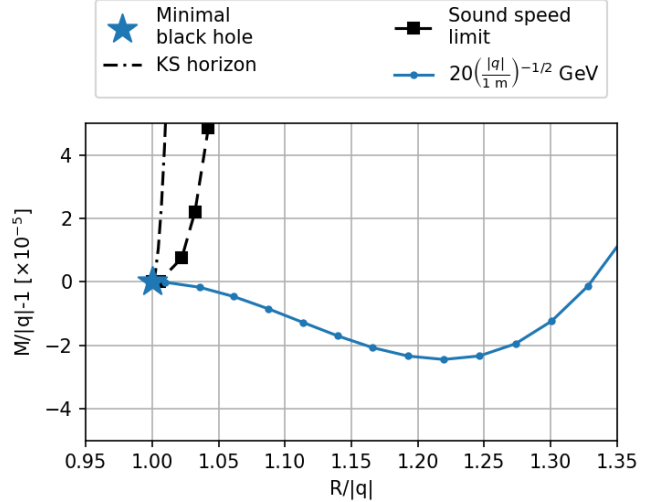


FIG. 4. Mass-radius profile of fermionic compact objects with fermion mass $m_f = 20(|q|/1 \text{ m})^{-1/2} \text{ GeV}$ near the minimal BH suggests a possible new state of compact object that is more compact than a NS. Sound speed limit is also depicted to show that this new compact objects does not exceed the sound speed limit.

far beyond the energy reach of any existing particle physics experiments.

It is noteworthy that the mass-radius curve shown in Fig. 1 converges toward the extreme point of $M = M_c$. This behavior is one of the key motivations of this work and it can be regarded as a distinctive feature of the KS solution in the deformed HL which exhibits a charged BH-like structure with two horizons. As shown in Figs. 2 and 3, both with and without interaction, a fermionic compact object with smaller fermion mass is similar to one in GR, whereas one with larger fermion mass is similar to the minimal BH in mass and radius. This is a drastically different feature compared to the GR case.

Another intriguing finding of this work is a possible existence of a new class of compact objects in HL gravity. We find that the compactness gap may be filled by fermionic compact objects with a fermion mass less than the given value in Table I. Fig. 4 shows the possibility of an additional branch of compact object which is smaller than NS both in mass and radius. Fixing $q \sim 1$ m for simplicity, one finds that the mass and radius of the most massive compact object with fermion mass 20 GeV without interaction ($y = 0$) are $\sim 10^{-3} M_\odot$ and ~ 20 m, respectively. For smaller radius, an additional peak appears in the mass-radius curve that is similar to the minimal BH in mass and radius. However, we do not observe this new class of compact object in the cases of $y > 0$, which may be attributed to the relatively coarse parameter set to reduce the computational cost. Nevertheless, there still remains the possibility that the interaction term could eliminate this new branch of compact objects. Further detailed investigation will be necessary to clarify this issue.

ACKNOWLEDGMENTS

The authors would like to thank Y.-M. Kim, M.-I. Park, K.Y. Kim, and J.W. Lee for the helpful discussion. This work is supported by the National Research Foundation of Korea (NRF) grants funded by the Ministry of Science and ICT (MSIT) of the Korea Government (NRF-2021R1A2C1093059, NRF-2020R1C1C1005863, RS-2025-

00555178). The work of K.K. is partially supported by the Korea Astronomy and Space Science Institute under the R&D program (Project No. 2026-1-810-00) supervised by the MSIT of the Korea Government. The work of E.J.S. and J.J.O. is partially supported by the National Institute for Mathematical Sciences under the Primary Research Program (Project No. B26720000) supported by the MSIT of the Korea Government.

[1] P. Hořava, *JHEP* **2009** (03), 020.

[2] P. Hořava, *Phys. Rev. D* **79**, 084008 (2009).

[3] P. Hořava, *Phys. Rev. Lett.* **102**, 161301 (2009).

[4] S. Mukohyama, *Class. Quant. Grav.* **27**, 223101 (2010).

[5] A. Kehagias and K. Sfetsos, *Phys. Lett. B* **678**, 123 (2009).

[6] H. Lü, J. Mei, and C. N. Pope, *Phys. Rev. Lett.* **103**, 091301 (2009).

[7] A. Wang, *Int. J. Mod. Phys. D* **26**, 1730014 (2017).

[8] M.-I. Park, *JHEP* **2009** (09), 123.

[9] K. Kim, J. J. Oh, C. Park, and E. J. Son, *Phys. Rev. D* **103**, 044052 (2021).

[10] J. R. Oppenheimer and G. M. Volkoff, *Phys. Rev.* **55**, 374 (1939).

[11] C. E. Rhoades, Jr. and R. Ruffini, *Phys. Rev. Lett.* **32**, 324 (1974).

[12] V. Kalogera and G. Baym, *Astrophys. J.* **470**, L61 (1996).

[13] N. Dadhich, *JCAP* **2020** (04), 035.

[14] A. Giuliani and T. Rothman, *Gen. Rel. Grav.* **40**, 1427 (2008).

[15] F. Özel, D. Psaltis, R. Narayan, and J. E. McClintock, *Astrophys. J.* **725**, 1918 (2010).

[16] M. Fishbach, R. Essick, and D. E. Holz, *Astrophys. J. Lett.* **899**, L8 (2020).

[17] M. Fishbach, *Science* **383**, 259 (2024).

[18] A. G. Abac, R. Abbott, I. Abouelfettouh, *et al.* (LIGO Scientific, KAGRA, VIRGO), *Astrophys. J. Lett.* **970**, L34 (2024).

[19] M. Fishbach, D. E. Holz, and W. M. Farr, *Astrophys. J. Lett.* **840**, L24 (2017).

[20] D. Gerosa and E. Berti, *Phys. Rev. D* **95**, 124046 (2017).

[21] B. Margalit and B. D. Metzger, *Astrophys. J.* **850**, L19 (2017).

[22] R. Abbott *et al.* (LIGO Scientific Collaboration and Virgo Collaboration), *Astrophys. J. Lett.* **913**, L7 (2020).

[23] M. Fishbach, W. M. Farr, and D. E. Holz, *Astrophys. J. Lett.* **891**, L31 (2020).

[24] M. Fishbach *et al.*, *Living Rev. Relativ.* **27**, 2 (2024).

[25] R. C. Tolman, *Phys. Rev.* **55**, 364 (1939).

[26] G. Narain, J. Schaffner-Bielich, and I. N. Mishustin, *Phys. Rev. D* **74**, 063003 (2006).

[27] S. Valdez-Alvarado, C. Palenzuela, D. Alic, and L. A. Ureña López, *Phys. Rev. D* **87**, 084040 (2013).

[28] P. Mukhopadhyay and J. Schaffner-Bielich, *Phys. Rev. D* **93**, 083009 (2016).

[29] M. Mariani, C. Albertus, M. d. R. Alessandroni, M. G. Orsaria, M. . Prez-Garca, and I. F. Ranea-Sandoval, *Mon. Not. R. Astron. Soc.* **527**, 6795 (2023).

[30] S. Deser, R. Jackiw, and S. Templeton, *Ann. Phys. (N.Y.)* **140**, 372 (1982).

[31] S. Deser, R. Jackiw, and S. Templeton, *Phys. Rev. Lett.* **48**, 975 (1982).

[32] E. J. Son, *Limits on the mass of compact objects in hořava-lifshitz gravity* (2026), arXiv:2601.03644 [gr-qc].

[33] W. Kim, E. J. Son, and M. Yoon, *JHEP* **2008**, 042 (2008).

[34] Y. S. Myung, *Phys. Lett. B* **685**, 318 (2010).

[35] J. Bellorin, A. Restuccia, and A. Sotomayor, *Phys. Rev. D* **90**, 044009 (2014).

[36] E. J. Son and W. Kim, *Phys. Rev. D* **83**, 124012 (2011).

[37] O. Gurtug and M. Mangut, *J. Math. Phys.* **59**, 042503 (2018).

[38] E. Hairer, G. Wanner, and S. P. Nørsett, Runge-kutta and extrapolation methods, in *Solving Ordinary Differential Equations I: Nonstiff Problems* (Springer Berlin Heidelberg, Berlin, Heidelberg, 1993) pp. 129–353.

[39] P. Virtanen, R. Gommers, T. E. Oliphant, M. Haberland, T. Reddy, D. Cournapeau, E. Burovski, P. Peterson, W. Weckesser, J. Bright, S. J. van der Walt, M. Brett, J. Wilson, K. J. Millman, N. Mayorov, A. R. J. Nelson, E. Jones, R. Kern, E. Larson, C. J. Carey, İ. Polat, Y. Feng, E. W. Moore, J. VanderPlas, D. Laxalde, J. Perktold, R. Cimrman, I. Henriksen, E. A. Quintero, C. R. Harris, A. M. Archibald, A. H. Ribeiro, F. Pedregosa, P. van Mulbregt, and SciPy 1.0 Contributors, *Nat. Methods* **17**, 261 (2020).

[40] A. Akmal, V. R. Pandharipande, and D. G. Ravenhall, *Phys. Rev. C* **58**, 1804 (1998).

[41] M. Oncins, *Constraints on pbh as dark matter from observations: a review* (2022), arXiv:2205.14722 [astro-ph.CO].

[42] M. Liu and J. Lu, *Phys. Lett. B* **699**, 296 (2011).